Design and evaluation of a novel breast cancer detection system combining both thermoacoustic (TA) and photoacoustic (PA) tomography

Manojit Pramanik, Geng Ku, Changhui Li, and Lihong V. Wang[a)]
Optical Imaging Laboratory, Department of Biomedical Engineering, Washington University in St. Louis, St. Louis, Missouri 63130

(Received 14 December 2007; revised 12 March 2008; accepted for publication 25 March 2008; published 6 May 2008)

We have developed a novel scanner for breast cancer detection, integrating both thermoacoustic and photoacoustic techniques to achieve dual contrast (microwave and light absorption) imaging. This scanner is nonionizing, low cost, and can potentially provide high-resolution, dual modality three-dimensional images of the breast. The scanner uses front instead of side breast compression and dry instead of gel ultrasonic coupling. Here we present the design of the breast scanner along with initial tissue phantom study results as a precursor to an actual patient study. © *2008 American Association of Physicists in Medicine*. [DOI: 10.1118/1.2911157]

I. INTRODUCTION

Breast cancer is currently the second leading cause of cancer deaths in women (after lung cancer) and is the most common cancer among women, excluding nonmelanoma skin cancers. One woman in eight either has or will develop breast cancer in her lifetime. In 2007, there were an estimated 178 480 new cases of breast cancer among females, and 2030 new cases among males. An estimated 40 460 females died of breast cancer, as did 450 males. Breast cancer is the most common cause of death in women between the ages of 45 and 55. Early diagnosis and treatment are the keys to surviving breast cancer.[1] With advances in screening, diagnosis, and treatment, the death rate for breast cancer has declined by about 20% over the past decade, and further research is ongoing to develop even more effective screening, diagnosis, and treatment programs.

Diagnosis of early breast cancer depends on the recognition of subtle changes in breast tissue properties, such as mechanical properties (hardness), optical absorption, radio frequency (rf) absorption (change in ion and water concentrations). Treatment is more likely to work well when cancer is found early. At present, x-ray mammography is the only mass screening tool used for detecting nonpalpable breast cancers. However, there are a few limitations of mammography.[2] The use of ionizing radiation (x ray) limits the frequency of mammographic screening. Despite using low doses of radiation, repeated x-ray exposure can cause problems. Further it is difficult to image dense glandular tissue and the region close to chest wall or underarm. And finally, very early stage tumors that do not yet exhibit microcalcifications cannot be imaged.

Sonographic examination of the breast has recently come to maturity with the advent of high-frequency multielement linear-array transducers. Ultrasonography is now routinely used in breast imaging centers as an essential complement to physical examination and mammography for the evaluation of breast masses, and as a tool to guide breast interventions. However, ultrasound specificity in breast cancer detection is limited by the overlapping acoustic characteristics of benign and malignant solid lesions (poor soft tissue contrast). Current ultrasound scanners can detect and resolve breast lesions a few millimeters in size. Ultrasound may miss tiny nonpalpable breast tumors because they have low acoustic contrast, or because of operator variability.[3]

Magnetic resonance imaging (MRI) offers improved tissue characterization over other imaging modalities. Contrast-enhanced MRI is increasingly used as a complementary diagnostic modality in breast imaging.[4] Although the sensitivity of breast MRI in the detection of malignancy has consistently been reported to be excellent, the specificity has been rather variable. Study protocols and imaging techniques are not standardized yet, and still there is a great deal of uncertainty about the role of MRI in clinical practice. Moreover, MRI is the most expensive of the current breast imaging modalities and requires the use of contrast agents which are not innocuous. Furthermore, conventional MRI gives only morphological information.

To overcome some of these difficulties, we have developed a breast screening modality that combines nonionizing radio frequency (rf) electromagnetic waves and a visible/near infrared (NIR) laser for the early breast cancer screening based on thermoacoustic/photoacoustic tomography (TAT/PAT). The rf contrast between malignant tumor tissue and normal human breast tissue is about a factor of 4.[5] A more recent study has shown the dielectric-properties contrast between malignant breast tissues and normal adipose-dominated breast tissues is large, ranging up to 10:1.[6] Extra water and sodium in the tumor tissue cause the enhanced dielectric property of the malignant tumor tissue.[7] The dielectric properties of malignant tumors show no significant variation with tumor age,[8] suggesting that a large contrast could exist even at earlier stages of tumor development. This large contrast is the primary motivation for our research on TAT, which measures the conductivity contrast. In comparisons, x-ray contrast is typically only a few percent among soft tissues. TAT combines the advantages of pure-ultrasound and pure-rf imaging.[9,10] Traditional imaging technology with pure ultrasound (ultrasonography) offers satisfactory spatial resolution but poor soft-tissue contrast,[11,12] pure-rf imaging provides good imaging contrast but poor spatial

resolution.[13–16] Despite its near-field operation, the best spatial resolution in pure-rf imaging is on the order of 10 mm, whereas the achievable resolution in pure-ultrasound while imaging is on the order of 1 mm. TAT bridges the gap between them by physically integrating ultrasound and rf and provides both satisfactory spatial resolution and high soft-tissue contrast. In fact, we have already demonstrated high-resolution (0.5 mm) deep tissue imaging using TAT.[17] The combined high resolution and high contrast holds promise for early breast cancer monitoring.

PAT overcomes the limitations of other optical modalities and combines optical contrast with ultrasonic resolution. In PAT, the contrast is related to the optical properties of the tissue, but the resolution is not limited by optical diffusion from multiple photon scattering. We have shown experimentally that the spatial resolution is bandwidth- and diffraction-limited by the photoacoustic waves because ultrasonic scattering is weak compared with optical scattering.[18,19] Optical technique is a unique noninvasive technology for imaging and quantifying vascularization, and especially oxygen saturation of breast tumors. These features are associated with angiogenesis and hypoxia, which are two correlates of breast malignancy. Furthermore, there is an intensified effort to produce extrinsic absorbing and fluorescent probes, especially for the NIR region, that target physiologic and genetic responses.[20–22] These probes could increase cancer contrast and target specific gene expression that could eventually improve early detection limits and specificity. The optical absorption contrast due to both oxy- and deoxy-hemoglobin relative to the background can be as high as 10:1 or even 100:1, depending on the optical wavelength.[23] Therefore, PA imaging may have a major role in breast cancer research and detection by assessing functional and molecular cancer characteristics.

I.A. Motivation for combining TAT and PAT

TAT and PAT are capable of giving additional information such as water/ion concentration, blood volume, and oxygenation level of hemoglobin. Because these parameters can change during the early stages of cancer, the combined TAT and PAT can potentially enhance early stage cancer diagnosis ability. Integrating the two modalities in a single system will have the following advantages: (1) It will reduce the image acquisition time, (2) it will be cost effective, and (3) acquiring two images in the same setup avoids moving and realigning the patient all over again. Moreover, TAT and PAT are both highly compatible with ultrasonography as they share the same ultrasound detection system. Therefore, in the future, ultrasound pulse-echo imaging can also be incorporated very easily into this system.

II. SYSTEM DESCRIPTION

In x-ray mammography the breast is compressed from the sides to reduce the thickness so that x-ray penetrates well. This compression causes some discomfort for the patient. Moreover, one needs to take a mammogram from different angles to interpret the images accurately. Our breast scanner is designed to minimize the compression pain. The breast is compressed from the front (nipple side) to give it a cylindrical shape. This technique has advantages in three ways. First, transducers can scan around the cylindrical breast for a full 360° and along the length to obtain a full three-dimensional (3D) data set. Full 3D reconstruction can be done to view the breast in 3D. Second, compression from the front is less painful than one from the side. Third, microwave/laser irradiation from the front of the cylindrically compressed breast can potentially penetrate deep enough to image near the chest wall.

A cylinder made out of low density polyethylene (LDPE), which has low ultrasound absorption and an acoustic impedance close to that of water (~1.5 at room temperature), holds the compressed breast. LDPE minimizes the loss of ultrasound signal due to a mismatched boundary. Figure 1(a) shows the schematic diagram of the scanner. The breast is inserted into the front opening of the scanner. A supporting plate made of acrylic pushes the breast from the rear opening of the scanner to obtain a cylindrical shape. After the compression, a brass retaining ring holds the supporting plate in position. The microwave/laser source is kept behind the scanner, and a horn antenna is pushed inside the scanner from the opening to irradiate rf/light on the compressed breast. An aluminum cylinder (rotating cylinder) with many holes holds the ultrasonic transducers around the breast holder cylinder. During data collection, the rotating cylinder is turned by a worm-gear mechanism and a stepper motor. The whole setup is mounted inside a stainless steel frame filled with mineral oil that facilitates the coupling of ultrasound to the transducer and also lubricates the worm gear. The scanner is placed on a height- and angle-adjustable metal frame. Figure 1(b) shows how a patient will be positioned, sitting on a chair and leaning onto the scanner.

The microwave/laser assembly is placed on the backside of the scanner behind the support plate. We illuminate the breast by either microwave or laser alternately for TAT/PAT. The microwave is delivered to the breast using a horn antenna, whereas the laser is delivered by a free space optical assembly. Some parts of the laser illumination system are incorporated inside the microwave horn antenna. As a result, we do not need to mechanically switch between the microwave and laser sources. The switching is electronic and instantaneous—once a TAT image is collected using microwave illumination, the microwave is switched off and the laser is switched on electronically to collect a PAT image. To be more precise, we have placed a prism and a ground glass plate inside the microwave horn antenna. Both are nonmetallic and therefore will not affect the microwave illumination. A drilled ~10-mm-diam hole in one narrow wall of the horn antenna delivers the light. The laser beam is broadened by a concave lens placed outside the hole on the horn antenna, then reflected by the prism, and homogenized by the ground glass. Figure 1(c) shows a schematic diagram of the integration of the light delivery through the horn antenna.

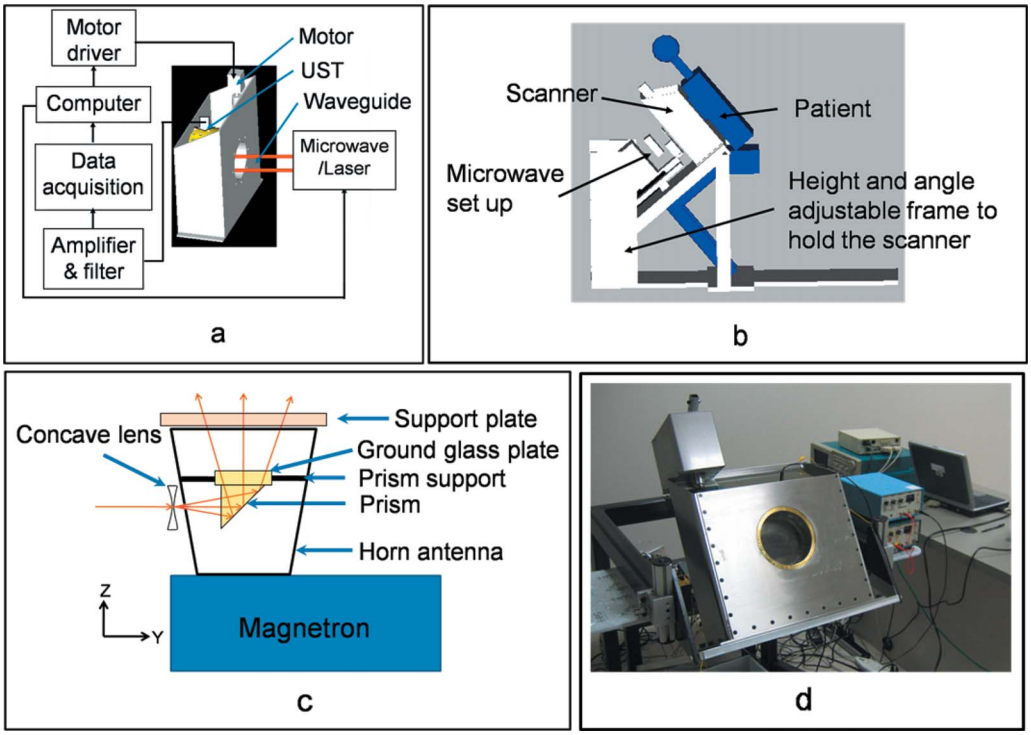

FIG. 1. Design of the system. (a) Schematic diagram of the breast scanner. UST: Ultrasonic Transducer. (b) The position of the patient with respect to the system. (c) Design of the integrated microwave horn antenna and optics. (d) Photograph of the system.

II.A. Microwave source

A 3.0 GHz microwave source produces pulses of width 0.5 μs (with a repetition rate of up to 40 Hz. The breast is illuminated using an air-filled pyramidal horn type antenna (WR284 horn antenna W/EEV flange, HNL Inc.) with an opening of 7.3×10.7 cm^2. The pulse energy is estimated to be around 10 mJ (=20 kW $\times$ 0.5 μs) (within the IEEE safety standards[24]). The support plate and the breast are separated from the opening of the antenna by about 1 cm, which is much less than the 10 cm microwave wavelength in air. Therefore most of the microwave energy either goes to the sample or gets reflected back to the horn antenna. Since the horn antenna is made of good conducting material with the only opening at the end facing the breast, most of the microwave energy is deposited into the breast even if microwave reverberation, due to impedance mismatch, exists between the breast and the horn antenna. Because the speed of the electromagnetic (EM) wave is so high, pulse broadening due to any reverberation is negligible. Therefore, the spatial resolution of TAT is not compromised.

The horn antenna is designed to transport the TE_{10} mode of EM waves, so the electric field is parallel (or nearly parallel for a horn) to the surface of either narrow side (y polarized in our system) and approaches zero near the inner surface of either narrow wall. By contrast, the electric field is nonzero near the surface of either wide wall. Therefore, opening the light delivery hole on the narrower side of the horn antenna (or waveguide) minimizes power leakage.

II.B. Laser source

A Q-switched Nd:yttrium–aluminum–garnet (YAG) laser with a repetition rate of 10 Hz provides 6.5-ns-wide (@1064 nm wavelength) laser pulses. The laser system can provide 850 mJ maximal output energy at 1064 nm wavelength. The laser is operated at this wavelength for maximum penetration into tissue. In this spectral region, absorption of melanin is relatively low and is not expected to limit the delivery of light into the breast, even for African American patients, as demonstrated in a previous study of diffuse optical imaging of the breast.[25] The laser beam is expanded by a concave lens, homogenized by a ground glass, and then directed onto the breast. This type of beam expansion scheme has been used extensively before.[17,26,27] The incident laser fluence on the tissue surface is controlled to <20 mJ/cm^2 to conform to the American National Standards Institute standards.[28]

II.C. Detection of ultrasound

For detecting the ultrasound signal, 13-mm/6-mm-diam active area nonfocused transducers operating at 2.25 MHz central frequency (ISS 2.25×0.5 COM, Krautkramer) are used. The transducers are scanned around the sample a full 360° to collect data at different angular positions. The signal is first amplified by a low-noise pulse amplifier (5072PR, OlympusNDT), then filtered electronically, and finally recorded using a digital data acquisition card (14 bit Gage Card). When microwave is the illumination source, a delay/

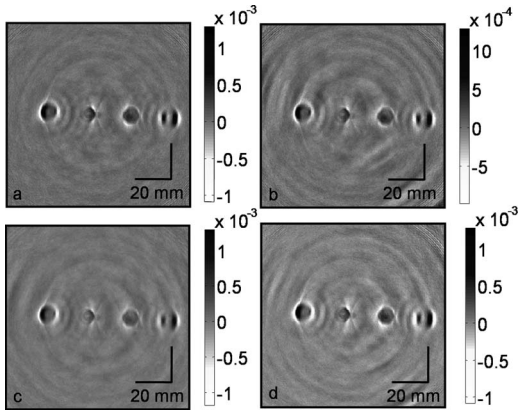

FIG. 2. Reconstructed TAT images acquired with (a) the intact horn antenna, (b) a prism mounted inside the horn antenna, (c) a 5-mm-diam hole drilled in a sidewall of the horn antenna, and (d) the hole in the sidewall and the prism mounted inside.

pulse generator (SRS, DG535) triggers the microwave pulses and synchronizes the data sampling of the Gage Card. On the other hand, during laser illumination the sync out of the laser system synchronizes the laser pulses and the data sampling of the Gage Card. Currently a two channel Gage Card is used for data collection thus two transducers are used simultaneously to get the data. In the future, we plan to use a 32 channel parallel data acquisition system. There are various reconstruction algorithms that can be used to reconstruct the PAT/TAT images from the raw data.[19,29–33] Here, a delay and sum (backprojection) algorithm is used for all image reconstruction. Figure 1(d) shows a photograph of the system.

III. RESULTS AND DISCUSSIONS

III.A. Integrating PAT/TAT

TAT and PAT have been separately used for tissue imaging by many groups.[9,17,29–31,34–39] However, these two modalities have never been combined before in a single system for breast imaging. To substantiate our new design of integrating optics with the microwave horn antenna, we performed the following experiment. Four water-based agar gel cylinders with ~10 mm diameter and ~10 cm length were placed inside a mineral oil bath, and images were acquired. Figure 2 shows the reconstructed images under different conditions. Figure 2(a) shows the original image with no optical device inside the microwave horn antenna. Figure 2(b) shows the image acquired when we put a prism inside the horn antenna. Figure 2(c) shows the image acquired after a hole of 5 mm diameter was drilled in the horn antenna, with no optical devices placed inside. Figure 2(d) shows the image obtained with the hole in the horn antenna and the prism placed inside. We can clearly see all four embedded objects with similar maximum signals (note that the gray scales are the same), except for some small background variations. From these four figures, we conclude that inserting the prism inside the horn antenna and drilling a hole in the sidewall do not cause much of signal loss or image distortion. These experimental results strongly support the placement of optical components (here, the prism and the ground glass plate) inside the horn antenna to deliver light, and as a result we are able to integrate both light and microwave delivery.

III.B. Dry coupling

Unlike conventional ultrasound imaging, where coupling gel is used between the body and the ultrasonic transducer,

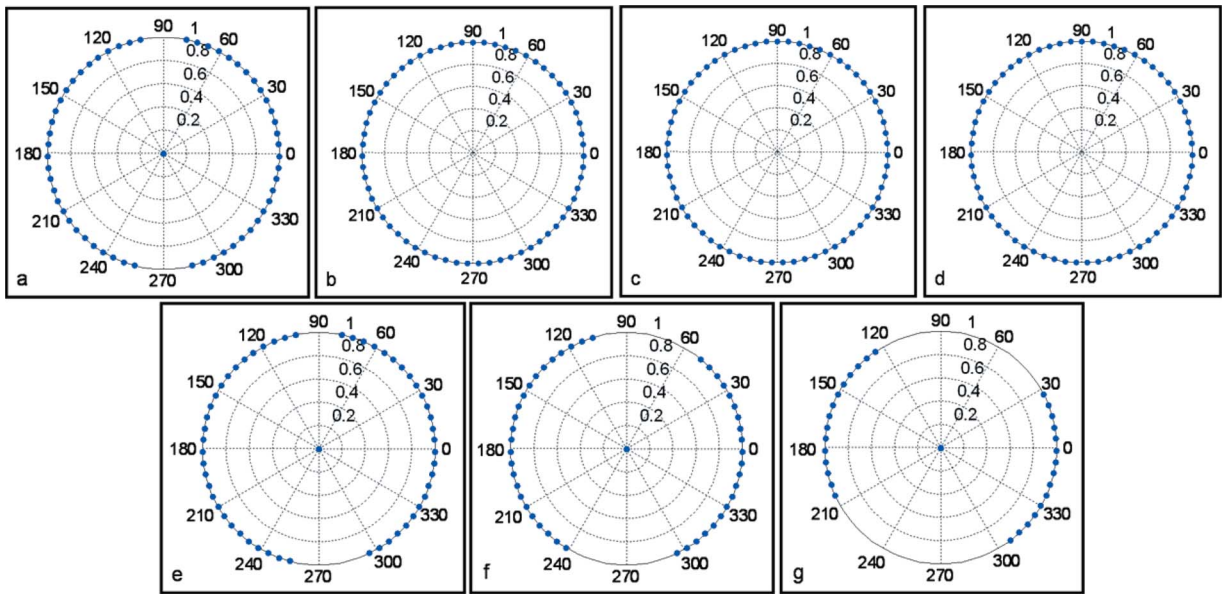

FIG. 3. The transmission of ultrasound around the breast holder at different depths with a compressed balloon filled with mineral oil inside the breast holder chamber. The dots represent the transmission of ultrasound in that region. Depths: (a) 9 mm, (b) 1.2 cm, (c) 3 cm, (d) 4.3 cm, (e) 4.6 cm, (f) 4.8 cm, and (g) 5 cm.

we will be using dry coupling. Since the cylindrically compressed breast will be held tightly inside the LDPE breast holder, there will not be a large air gap to hinder ultrasound propagation. To test the feasibility of dry coupling we have used a thin rubber balloon filled with mineral oil as a breast model. We put the balloon inside the breast holder chamber and then compressed it to a cylindrical shape that fit tightly inside the LDPE breast holder cylinder. This experiment was done with the scanner tilted at 45°. There was a little bit of air gap at the top portion of the breast holder cylinder. Even with this little air gap between the balloon and the breast holder cylinder, when we made a transmission ultrasound measurement around the breast holder cylinder we saw very good ultrasound coupling. Figure 3 shows the transmission ultrasound coupling at different depths of the compressed balloon.

From Fig. 3 we can see that, except near the two ends of the compressed balloon [Figs. 3(a) and 3(g)], the remaining planes have quite good ultrasonic transmission, which means we have good ultrasonic coupling. Even for those few planes where we do not have good coupling, we have good coupling over 80% of the area. Since we do tomography and collect data at different angular positions for reconstruction, losing data over 20% of the area will not affect the reconstructed image.

III.C. Phantom experiments

We tested our system using tissue phantoms. Porcine fat was used as the background medium mimicking the fatty breast tissue, and water-based agar gel was used to model the inhomogeneity (target) in the background. The target gel objects were made of 2% agar, 2% salt and 96% water. Salt was added to increase the microwave absorption. A total of five target objects of diameter ~6 mm were buried inside ~7-cm-diam porcine fat. Two targets were made of clear gel. The remaining three targets were made of black gel; the color was obtained by mixing black India ink during the preparation of the agar gel. The location of the target objects inside the base fat is shown in Fig. 4(a), a photograph of the phantom. The rf absorption contrast between the target gel and the background fat tissue is estimated to be ~4:1. The optical contrast between the black target gel and background fat tissue is estimated to be ~5:1. Both microwave and optical contrast are in the similar range of what we can expect in real human breast. The sample was placed inside the breast holder chamber, and the chamber was then filled with mineral oil, an ultrasound coupling medium. The sample was first illuminated with microwave and then by a 1064 nm wavelength laser.

Figures 4(b) and 4(c) show the reconstructed TAT images with 13- and 6-mm-diam active area ultrasonic transducers, respectively. The contrast and signal-to-noise (SNR) in the reconstructed images are ~3.5:1 and 34, respectively, for a 13-mm-diam transducer [Fig. 4(b)] and the same numbers for a 6-mm-diam transducer are ~2.5:1 and 20, respectively [Fig. 4(c)]. The resolution is calculated to be ~1.2 and ~0.7 mm for the images obtained by 13- and 6-mm-diam

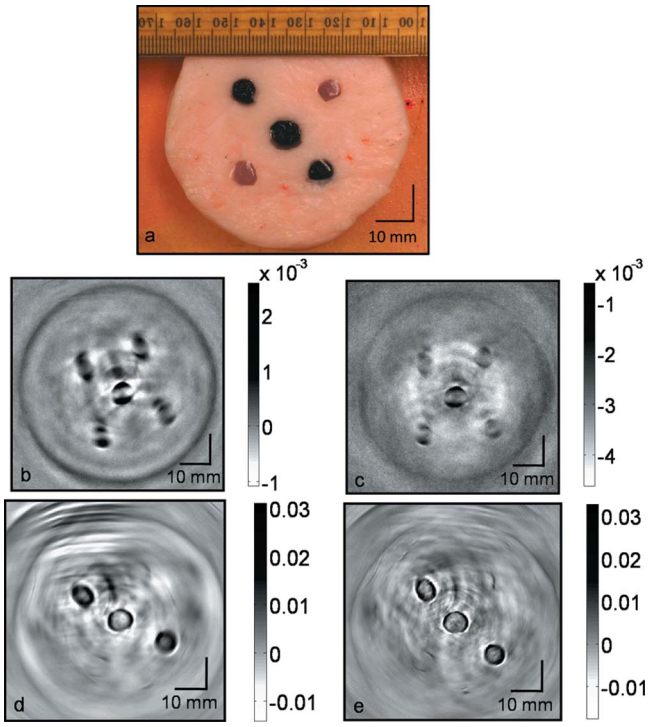

FIG. 4. Cross-sectional TAT and PAT images of tissue mimicking phantom obtained from the scanner. Five water-based agar gel targets were embedded inside a porcine fat base. (a) Photograph of the phantom. Two targets were clear objects and the other three targets were black. (b) TAT image obtained using 13-mm-diam active area transducer. (c) TAT image obtained using 6-mm-diam active area transducer. (d) PAT image obtained at 1064 nm wavelength using a 13-mm-diam active area transducer. (e) PAT image obtained at 1064 nm wavelength using a 6-mm-diam active area transducer.

transducers, respectively. Distortion of the TAT images is noted. Although the target object has a circular cross section, the reconstructed images from TAT appear to be split into two objects [Fig. 2, Fig. 4(b), and Fig. 4(c)]. Various factors such as the target object size, conductivity of the target objects, and microwave diffraction contribute to the image distortion. We have reported this phenomenon in detail in another journal paper.[40] Figures 4(d) and 4(e) show PAT images with 13- and 6-mm-diam active area transducers, respectively. The contrast and SNR in the reconstructed images are ~4.1:1 and 64, respectively, for the 13-mm-diam transducer [Fig. 4(d)] and the same numbers for the 6-mm-diam transducer are ~3.8:1 and 27, respectively [Fig. 4(e)]. The resolution of the images obtained by both the transducers is calculated to be ~0.7 mm.

As expected, we can clearly see all five objects in the TAT images [Figs. 4(b) and 4(c)]. TAT is based on microwave absorption and all five objects are made of water-based gel that is much more opaque to microwave than the background fat tissue. In contrast, PAT images reveal only three black target objects as the contrast in PAT imaging is dependent on light absorption coefficient. Thus the combination of both PAT and TAT will provide us with more information about the target objects.

IV. CONCLUSIONS

TAT and PAT together can provide additional functional information for the diagnosis of breast cancer. We have successfully integrated the two imaging modalities into one system, making it easier to get an image at the same time. Our system should be much more comfortable for the patient, and we will not need to apply gel or other chemicals on the skin: our system operates with dry coupling. We have also achieved good quality PAT and TAT images on tissue mimicking phantoms. In the future, pure ultrasound pulse-echo images can also be obtained in this modality. Thus we are able to provide multimodality, high resolution, high contrast, and low cost breast images which can be potentially used for early breast cancer detection.

ACKNOWLEDGMENTS

We thank Xiao Xu for experimental assistance with the laser, and also acknowledge the support provided by National Institutes of Health Grant Nos. R01 EB000712 and R01 NS046214.

[a]Author to whom correspondence should be addressed. Electronic mail: Lhwang@biomed.wustl.edu

[1]J. R. Harris *et al.*, "Medical progress: Breast cancer," N. Engl. J. Med. **327**(6), 390–398 (1992).
[2]S. J. Nass, I. C. Henderson, and J. C. Lashof, *Mammography and Beyond: Developing Techniques for the Early Detection of Breast Cancer* (Inst. Med., Nat. Acad. Press, Washington, D.C., 2001).
[3]C. D. Lehman *et al.*, "Cancer yield of mammography, MR, and US in high-risk women: Prospective multi-institution breast cancer screening study," Radiology **244**(2), 381–388 (2007).
[4]C. Kuhl, "The current status of breast MR imaging—Part I. Choice of technique, image interpretation, diagnostic accuracy, and transfer to clinical practice," Radiology **244**(2), 356–378 (2007).
[5]S. Chaudhary *et al.*, "Dielectric properties of normal and malignant human breast tissues at radiowave and microwave frequencies," Indian J. Biochem. Biophys. **21**, 76–79 (1984).
[6]M. Lazebnik *et al.*, "A large-scale study of the ultrawideband microwave dielectric properties of normal, benign and malignant breast tissues obtained from cancer surgeries," Phys. Med. Biol. **52**(20), 6093–6115 (2007).
[7]Freddy Homburger, *The Physiopathology of Cancer*, 2nd ed. (Hoeber-Harper, New York, 1959).
[8]A. Swarup, S. S. Stuchly, and A. Surowiec, "Dielectric-properties of mouse Mcal fibrosarcoma at different stages of development," Bioelectromagnetics (N.Y.) **12**(1), 1–8 (1991).
[9]L. H. V. Wang *et al.*, "Microwave-induced acoustic imaging of biological tissues," Rev. Sci. Instrum. **70**(9), 3744–3748 (1999).
[10]R. A. Kruger *et al.*, "Breast cancer in vivo: Contrast enhancement with thermoacoustic CT at 434 MHz—Feasibility study," Radiology **216**(1), 279–283 (2000).
[11]Frederick W. Kremkau *Diagnostic Ultrasound: Principles and Instruments*, 4th ed. (Saunders, Philadelphia, 1993).
[12]E. Steen and B. Olstad, "Volume rendering of 3-D medical ultrasound data using direct feature mapping," IEEE Trans. Med. Imaging **13**, 517–525 (1994).
[13]J. C. Lin, "Frequency optimization for microwave imaging of biological tissues," Proc. IEEE **73**, 374–375 (1985).
[14]Lawrence E. Larsen, John H. Jacobi, and IEEE Microwave Theory and Techniques Society, *Medical Applications of Microwave Imaging* (IEEE Press, New York, 1986).
[15]E. C. Fear and M. A. Stuchly, "Microwave system for breast tumor detection," IEEE Microw. Guid. Wave Lett. **9**(11), 470–472 (1999).
[16]J. H. Jacobi and L. E. Larsen, "Microwave time delay spectroscopy imagery of isolated canine kidney," Med. Phys. **7**, 1–7 (1980).
[17]G. Ku *et al.*, "Thermoacoustic and photoacoustic tomography of thick biological tissues toward breast imaging," Technol. Cancer Res. Treat. **4**(5), 559–565 (2005).
[18]M. H. Xu and L. V. Wang, "Analytic explanation of spatial resolution related to bandwidth and detector aperture size in thermoacoustic or photoacoustic reconstruction," Phys. Rev. E **67**(5), 056605 (2003).
[19]M. H. Xu and L. H. V. Wang, "Pulsed-microwave-induced thermoacoustic tomography: Filtered backprojection in a circular measurement configuration," Med. Phys. **29**(8), 1661–1669 (2002).
[20]K. Licha *et al.*, "Hydrophilic cyanine dye as contrast agents for near-infrared tumor imaging: Synthesis, photophysical properties, and spectroscopic in vivo characterization," Photochem. Photobiol. **72**(3), 392–398 (2000).
[21]S. Achilefu *et al.*, "Novel receptor-targeted fluorescent contrast agents for in vivo tumor imaging," Invest. Radiol. **35**(8), 479–485 (2000).
[22]R. Weissleder *et al.*, "In vivo imaging of tumors with protease-activated near-infrared fluorescent probes," Nat. Biotechnol. **17**(4), 375–378 (1999).
[23]L. V. Wang and H.-i. Wu, *Biomedical Optics: Principles and Imaging* (Wiley, New York, 2007).
[24]IEEE standard for safety levels with respect to human exposure to radio frequency electromagnetic fields 3 kHz to 300 GHz, IEEE Std C95.1, 1999 Edition.
[25]B. Monsees, J. M. Destouet, and W. G. Totty, "Light scanning versus mammography in breast cancer detection," Radiology **163**, 463–465 (1987).
[26]G. Ku and L. H. V. Wang, "Deeply penetrating photoacoustic tomography in biological tissues enhanced with an optical contrast agent," Opt. Lett. **30**(5), 507–509 (2005).
[27]Y. W. Wang *et al.*, "Photoacoustic tomography of a nanoshell contrast agent in the in vivo rat brain," Nano Lett. **4**(9), 1689–1692 (2004).
[28]Laser Institute of America, American National Standard for Safe Use of Lasers ANSI Z136.1-2000 (American National Standards Institute, Inc., New York, NY, 2000).
[29]M. H. Xu and L. H. V. Wang, "Time-domain reconstruction for thermoacoustic tomography in a spherical geometry," IEEE Trans. Med. Imaging **21**(7), 814–822 (2002).
[30]Y. Xu, D. Z. Feng, and L. H. V. Wang, "Exact frequency-domain reconstruction for thermoacoustic tomography - I: Planar geometry," IEEE Trans. Med. Imaging **21**(7), 823–828 (2002).
[31]Y. Xu, M. H. Xu, and L. H. V. Wang, "Exact frequency-domain reconstruction for thermoacoustic tomography - II: Cylindrical geometry," IEEE Trans. Med. Imaging **21**(7), 829–833 (2002).
[32]M. H. Xu, Y. Xu, and L. H. V. Wang, "Time-domain reconstruction-algorithms and numerical simulations for thermoacoustic tomography in various geometries," IEEE Trans. Biomed. Eng. **50**(9), 1086–1099 (2003).
[33]M. H. Xu and L. H. V. Wang, "Photoacoustic imaging in biomedicine," Rev. Sci. Instrum. **77**(4), 1–22 (2006).
[34]R. A. Kruger *et al.*, "Thermoacoustic CT with radio waves: A medical imaging paradigm," Radiology **211**(1), 275–278 (1999).
[35]R. A. Kruger and W. L. Kiser, Jr., "Thermoacoustic CT of the breast: Pilot study observations," Proc. SPIE **4256**, 1–5 (2001).
[36]G. Ku and L. H. V. Wang, "Scanning microwave-induced thermoacoustic tomography: Signal, resolution, and contrast," Med. Phys. **28**(1), 4–10 (2001).
[37]X. D. Wang *et al.*, "Noninvasive laser-induced photoacoustic tomography for structural and functional in vivo imaging of the brain," Nat. Biotechnol. **21**(7), 803–806 (2003).
[38]G. Ku *et al.*, "Imaging of tumor angiogenesis in rat brains in vivo by photoacoustic tomography," Appl. Opt. **44**(5), 770–775 (2005).
[39]A. A. Oraevsky *et al.*, "Optoacoustic imaging of blood for visualization and diagnostics of breast cancer," Proc. SPIE **4618**, 81–94 (2002).
[40]C. Li *et al.*, "Image distortion in thermoacoustic tomography caused by microwave diffraction," Phys. Rev. E **77**(3), 031923 (2008).